applied sciences

MDPI

Article

Mechanical and Electrical Properties of DNA Hydrogel-Based Composites Containing Self-Assembled Three-Dimensional Nanocircuits

Ming Gao [1], Abhichart Krissanaprasit [1], Austin Miles [2], Lilian C. Hsiao [3] and Thomas H. LaBean [1,*]

[1] Department of Materials Science and Engineering, College of Engineering, North Carolina State University, Raleigh, NC 27695, USA; mgao4@ncsu.edu (M.G.); akrissa@ncsu.edu (A.K.)
[2] North Carolina School of Science and Mathematics, Durham, NC 27705, USA; austinmiles57@gmail.com
[3] Department of Chemical and Biomolecular Engineering, College of Engineering, North Carolina State University, Raleigh, NC 27695, USA; lilian_hsiao@ncsu.edu
* Correspondence: thlabean@ncsu.edu; Tel.: +1-919-515-2204

Abstract: Molecular self-assembly of DNA has been developed as an effective construction strategy for building complex materials. Among them, DNA hydrogels are known for their simple fabrication process and their tunable properties. In this study, we have engineered, built, and characterized a variety of pure DNA hydrogels using DNA tile-based crosslinkers and different sizes of linear DNA spacers, as well as DNA hydrogel/nanomaterial composites using DNA/nanomaterial conjugates with carbon nanotubes and gold nanoparticles as crosslinkers. We demonstrate the ability of this system to self-assemble into three-dimensional percolating networks when carbon nanotubes and gold nanoparticles are incorporated into the DNA hydrogel. These hydrogel composites showed interesting non-linear electrical properties. We also demonstrate the tuning of rheological properties of hydrogel-based composites using different types of crosslinkers and spacers. The viscoelasticity of DNA hydrogels is shown to dramatically increase by the use of a combination of interlocking DNA tiles and DNA/carbon nanotube crosslinkers. Finally, we present measurements and discuss electrically conductive nanomaterials for applications in nanoelectronics.

Keywords: DNA hydrogel; DNA hydrogel-based composites; self-assembly; biomaterials; DNA nanotechnology; carbon nanotubes; gold nanoparticles

Citation: Gao, M.; Krissanaprasit, A.; Miles, A.; Hsiao, L.C.; LaBean, T.H. Mechanical and Electrical Properties of DNA Hydrogel-Based Composites Containing Self-Assembled Three-Dimensional Nanocircuits. *Appl. Sci.* **2021**, *11*, 2245. https://doi.org/10.3390/app11052245

Academic Editor: Alexander Marras

Received: 5 February 2021
Accepted: 24 February 2021
Published: 3 March 2021

1. Introduction

Self-assembly by molecular recognition is a fundamental property of soft matter that can be utilized as a building tool to construct nanoscale to macroscale materials via bottom-up approaches. Using programmed assembly of nucleic acid molecules, structural DNA nanotechnology has rapidly expanded to construct sophisticated biomaterials [1–5]. Beyond self-assembly, DNA is also biocompatible and can be readily conjugated with other bio-/nanomaterials including proteins and conductive polymers [6–9]. Leveraging these capabilities, DNA-based hydrogels have drawn a lot of attention starting with basic research and moving to applications such as biomedicine, biosensing, and drug delivery [10–15].

The most common strategies to form DNA-based hydrogels are through complementary strand hybridization, enzyme-catalyzed assembly, and molecular entanglement [16]. Studies based extensively upon hybridization focused mainly on pure DNA hydrogels with three-dimensional (3D) hydrophilic networks crosslinked via complementary basepairing. These hydrogels typically employed multistrand DNA tiles to construct the multivalent, crosslinking structural members (crosslinkers) as well as the spacer units (spacers) designed to assemble and control spacing between adhesive arms of the crosslinkers [17,18]. DNA hydrogels contain available free volume between their polymeric chains in which other nanomaterials can be trapped, thus providing them the capacity to non-specifically incorporate functional components. Recently, studies have described strategies for coating

and crosslinking nanomaterials such as quantum dots, nanoparticles, and nanotubes with DNA to create a variety of water soluble heterostructured conjugates [19–21]. Using these DNA/nanomaterial conjugates as integral building blocks of crosslinked molecular networks has led to interesting DNA hydrogel composites assembled with oligonucleotides and other nanomaterials.

Integration of nanomaterial conjugates makes it possible to modify the hydrogel properties to engineer mechanically and electrically adjustable materials. The mechanical properties of hydrogel-based composites can be fine-tuned by adjusting the concentrations and branch architectures of initial DNA tiles and embedded nanomaterials. However, the electrical properties of hydrogel composites bearing embedded conductive nanomaterials have rarely been studied, and there is a need for a deeper understanding of DNA as a building material to assemble 3D nanocircuits with conductive nanomaterials. One such material is carbon nanotubes (CNTs). CNTs are known for their utility in reinforcing nanofiber networks due to their excellent mechanical strength and stiffness [22]. They are chemically stable and have high aspect ratios that contribute to electrical percolation in nanocomposites, which makes CNTs a promising material in nanoelectronics applications [23]. However, bare CNTs naturally have low solubility in aqueous solutions in the absence of surfactants or sidewall functionalizations [24]. One method to effectively solubilize CNTs is via biomolecular dispersion, where single-stranded DNA (ssDNA) wraps around individual nanotubes via the strong non-covalent hydrophobic interactions between CNT walls and DNA nucleobases to form water-soluble supramolecular complexes [25–28]. Besides improving solubility and manageability, the DNA–CNT hybrids also combine the advantageous electrical and mechanical properties of CNTs and the molecular recognition capabilities of DNA. Moreover, CNTs have been a promising material for the development of non-volatile memory with short switching times [29]. Some CNT-based memory has been shown to operate using electromechanical interactions of nanotubes with each other under the influence of an applied voltage [30]. For this reason, researchers have chosen CNTs to build memristive structures; these are structures that display variable electrical resistance based upon their ability to remember recent current/voltage activity. Another classic example of integrating biomolecules with nanomaterials is DNA-functionalized gold nanoparticles (AuNPs). These hybrids have been shown to be useful for many applications from biosensing to use as building blocks with which to fabricate more complicated nanostructures [31,32]. The original approach to make DNA–AuNP conjugates is to bind thiolated DNA to AuNPs with the formation of gold–thiolate bonds [33,34]. More recently, another strategy has been reported to adsorb non-thiolated DNA strands onto AuNPs via polyadenine bases that interact strongly with the gold surface [35]. Since this method covers AuNP surfaces quickly and effectively with unmodified ssDNA and provides an acceptable loading capacity, it was adapted in our study for synthesis of DNA-functionalized AuNPs.

Here, we present the construction and analysis of DNA hydrogels, some with embedded percolating networks using DNA-wrapped CNTs and DNA-attached AuNPs as crosslinkers. We started at the molecular level by designing DNA sequences and moved up to macroscale hydrogels realized by bottom-up fabrication. We applied the crosslinker plus spacer design, where oligonucleotides were designed to form molecular networks by sequence-directed hybridization with sticky ends on crosslinker units (i.e., DNA tiles or DNA/nanomaterial conjugates) and coupling components (i.e., spacers) to construct 3D networks (Figure 1). We were able to improve the mechanical strength of the formed hydrogels using a variety of strategies including adjusting the spacer length and mixing different types of crosslinkers. We also showed that the 3D structures of nanomaterials can be programmed efficiently via nucleic acid sequence, and that it is possible to direct the formation of percolating networks with DNA self-assembly. In addition, using inspiration from biological neural networks that display extraordinary signal dynamics and processing abilities, we aimed to mimic some aspects of the morphology of natural neural networks using DNA self-assembly to fabricate nanoelectronic devices with measurable function. Non-linear electrical properties of nanocomposites that integrate DNA-modified

CNTs are reported. Our eventual goal is to harness molecular recognition to precisely control the configuration and connection of nanomaterials to self-assemble into controllable nanostructures and, thus, to engineer, fabricate, and characterize DNA-based hydrogels for desired applications. Future DNA hydrogel composites may find impactful application as building blocks in artificial computer hardware, with architectures inspired by natural neural systems for memory and information-processing applications.

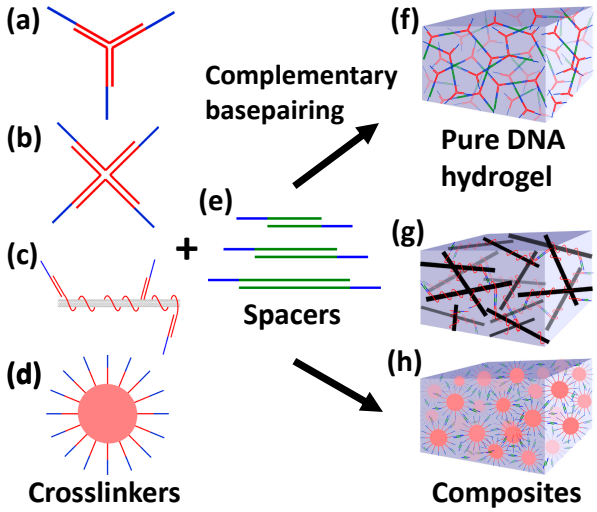

Figure 1. Schematic illustrations of DNA-based hydrogel formation. (**a**–**d**) Various types of crosslinkers: (**a**) Y-shaped DNA tile, (**b**) X-shaped DNA tile, (**c**) DNA–carbon nanotube (CNT) conjugate, and (**d**) DNA–gold nanoparticle (AuNP) conjugate. (**e**) Spacers of different lengths: Ss, Sm, and Sl (short (33 nt), medium (44 nt), and long (55 nt), respectively). (**f**) Pure DNA hydrogel constructed by combining Y-shaped or X-shaped DNA tiles with spacers. (**g**,**h**) DNA hydrogel composites: (**g**) DNA–CNT hydrogel and (**h**) DNA–AuNP hydrogel.

2. Materials and Methods

Materials. Oligonucleotides were purchased from Integrated DNA Technologies (IDT, Coralville, IA, USA). Oligonucleotides were ordered with standard desalting, and no further purification was performed prior to use. Nucleotide sequences are listed in Supplementary Table S1. Single-walled carbon nanotubes (SWNTs; 0.78 nm average diameter; 1 μm median length) were purchased from Sigma-Aldrich (773735, St. Louis, MO, USA), and multi-walled carbon nanotubes (MWNTs) were purchased from Sigma-Aldrich (698849). Milli-Q deionized (DI) water (>18 MΩ·cm resistivity) was used for all experiments. Nitric acid (ACS reagent, Sigma-Aldrich) and hydrochloric acid (ACS reagent, Sigma-Aldrich) were used to make aqua regia. Hydrogen tetrachloroaurate (III) trihydrate (99.9%, Sigma-Aldrich) and sodium citrate tribasic dihydrate (ACS reagent, >99.0%, Sigma-Aldrich) were purchased for the synthesis of gold nanoparticles. In addition, Tris base (tris(hydroxymethyl)aminomethane, Fisher Scientific), sodium chloride (NaCl, >99.5%, Sigma-Aldrich), HEPES (4-(2-hydroxyethyl)-1-piperazineethanesulfonic acid) (>99.5%, Sigma-Aldrich), and sodium hydroxide (NaOH, >98%, Sigma-Aldrich) were used to make buffer solutions.

Synthesis of gold nanoparticles (AuNPs). AuNPs were synthesized based on a method adapted from the standard citrate reduction procedures [36]. First, all glassware was cleaned with aqua regia and then rinsed with DI water. After the glassware was dried completely, 500 mL of 1 mM hydrogen tetrachloroaurate (III) trihydrate in DI water was prepared in a round-bottom flask and heated to a vigorous boil with stirring. Then, 50 mL of 38.8 mM sodium citrate tribasic dihydrate in DI water was added to the gold solution flask and the reaction was allowed to proceed for 15 min. The solution turned from yellow to clear, to black, to purple, and finally to deep red. Lastly, the solution was cooled down to room temperature. Synthesized AuNPs were characterized by transmission

electron microscopy (TEM). The concentration of AuNPs was estimated with a UV–Vis spectrophotometer and calculated using the Beer–Lambert equation, $A = \varepsilon bC$ [37].

Construction of DNA tiles and spacers. To construct Y-shaped DNA tiles, 10 µL of 10 mM Y_1, Y_2, and Y_3 precursor strands for the building blocks was added to a folding buffer solution (20 mM Tris-HCl (pH 7.5) and 100 mM NaCl) to obtain a final concentration of 1 mM for each strand. Then, the mixture went through a heat-annealing process where it was heated to 95 °C for 5 min and then cooled to room temperature over 30 min. Similarly, the X-shaped DNA tiles were assembled by mixing 8 µL of 10 mM precursor strands X_1, X_2, X_3, and X_4 in the folding buffer solution to obtain a final concentration of 1 mM for each strand. The mixture went through the same heat-annealing process as described above. To construct spacers, 15 µL of the two 10 mM precursor strands for the spacers was mixed in the folding buffer (to obtain a final concentration of 1.5 mM for each strand). The mixture then went through the same heat-annealing process described above for DNA tiles. Spacers were also made to different concentrations to pair with different types of crosslinkers. All pH values of the buffers were measured with a standard pH meter (Mettler Toledo SevenEasy™, Columbus, USA).

DNA-assisted solubilization of CNTs and DNA–CNT conjugate formation. We constructed DNA–CNT conjugates by wrapping CNTs with DNA based on a previously reported method [38]. Briefly, 120 µL HEPES (final concentration 50 mM, pH 7.6), 1.2 mg CNTs, and 15 µL of 10 mM DNA strand C_1 were mixed together. The mixture was sonicated in an ice-water bath for 30 min using a 100-W bath sonicator. Then, 15 µL of 10 mM DNA strand C_2 was added. The solution was incubated at room temperature overnight and then stored at 4 °C.

DNA–AuNP conjugates. DNA-decorated AuNPs were synthesized with a previously reported method [39]. First, 16 µL of DNA stock solution of sequence G (100 µM in 5 mM HEPES buffer, pH 7.4) was added to 1.6 mL AuNP solution (10 nM). The solution was mixed by brief vortexing. Then, 32 µL of 500 mM citrate·HCl buffer, pH 3 (final 10 mM), was added to the AuNP solution (1 µL of buffer per 50 µL of AuNP solution). The solution once again went through vortex mixing and was incubated at room temperature for 3 min. Then, the pH of the AuNP solution was adjusted back to neutral by adding 96 µL of 500 mM HEPES buffer (pH 7.6, 3 µL of buffer per 50 µL of AuNP solution). The solution was then incubated for 5 to 10 min at room temperature. The DNA–AuNP mixture was centrifuged at 13,300 rpm for 6 min, and the supernatant was removed and discarded. The pellet was washed four times with 5 mM HEPES buffer (pH 7.6) and centrifuged to remove any unbound DNA strands. The final DNA–AuNP conjugate was redispersed in 100 µL of 5 mM HEPES buffer (pH 7.6) for further use.

Construction of pure and DNA hydrogel composites. To make hydrogels using the self-assembled DNA tiles or DNA/nanomaterials conjugates, and spacers, desired volumes of crosslinker and spacer stocks were combined on a piece of parafilm using the concentrations and ratios listed in Table S2. For example, 10 µL of Y-shaped DNA tiles stock and 10 µL of spacer stock were added on a piece of parafilm and immediately mixed. DNA hydrogels were formed within one minute, and the DNA gel samples were immediately tested.

TEM and analysis. The dimensions and morphology of AuNPs, DNA–AuNP conjugates, DNA–CNT conjugates, and dehydrated DNA hydrogel composites were imaged using an FEI Talos F200X scanning/transmission electron microscope (Hillsboro, OR, USA) at an accelerating voltage of 200 kV. CNT samples were drop cast and dried onto 300-mesh copper grids with lacey formvar support film reinforced by a heavy coating of carbon (Ted Pella, 01883, Redding, USA). AuNP samples were prepared on 200-mesh copper grids with a formvar film covered with a light layer of carbon (Ted Pella, 01800-F). Dimensions of the imaged samples were measured with ImageJ software (Bethesda, MD, USA).

Measurement of rheological properties of hydrogels. A TA Instruments DHR-2 stress-controlled rheometer (New Castle, DE, USA) was used to perform small-amplitude oscillation frequency sweeps at room temperature. An aluminum plate of 20-mm diameter

was used as the top plate. We prepared DNA hydrogel samples by pipetting the components onto parafilm; following gel formation, the samples were transferred to the rheometer plate without pipetting, to avoid shearing the gels. For a ~30-µL hydrogel sample, the gap distance was set as 35 µm. The applied strain was set to 1%, while the angular frequency was decreased from 100 to 0.1 rad/s. Five points were collected per decade.

Electrodes and electrical measurement setup. Gold electrodes of parallel lines with defined widths and gap distances were fabricated via thin film vapor deposition. To perform current–voltage (IV) curve measurement, the sample was connected to a socket board in a Faraday cage (Hewlett Packard Test Fixture Analyzer 16058A, Palo Alto, CA, USA) connected to a 2-channel (medium power) source/monitor unit module (Agilent Technologies E5272A, Santa Clara, CA, USA).

3. Results

3.1. Sequence Design of Crosslinker and Spacer Strands for DNA Gel Formations

We constructed DNA hydrogels by mixing crosslinker and spacer modules that associate based on DNA–DNA hybridization, as shown in Figure 1. Four types of crosslinkers (Y-shaped DNA tiles, X-shaped DNA tiles, DNA–CNT conjugates, and DNA–AuNP conjugates) and three different lengths of spacers (Ss, Sm, and Sl; short (33 nt), medium (44 nt), and long (55 nt), respectively) were tested. With these building blocks, we produced two major types of hydrogels: pure DNA hydrogels and DNA/nanomaterial hydrogel composites. For DNA crosslinkers, we used two types of branching crosslinkers called Y-shaped and X-shaped DNA tiles that were assembled from three and four ssDNA strands, respectively. Each arm in the DNA tile carried a sticky end complementary to sticky ends on the spacers. We adopted sequences of strands D_1, D_2, and D_3 from Xing et al. to construct Y-shaped DNA tiles [40]. Similarly, we modified the sequences of strands X_{01}, X_{02}, X_{03}, and X_{04} reported by Um et al. [41] by swapping in our sticky end to construct X-shaped DNA tiles.

To construct DNA–CNT conjugates, we applied a DNA sequence containing multiple repeated GT units that wrap around CNTs. Specifically, we adopted Sequence C as reported by Cheng et al. [38] and modified their Sequence D with our sticky end to make it compatible with our spacers. The repeated GT units have been proven to efficiently wrap around CNTs well due to strong π–π interactions between the CNT sidewall and the nucleobase aromatic rings [38,42]. Zheng et al. also demonstrated a systematic study showing that among all DNA sequences that wrap around CNTs, $(GT)_n$ gives the highest dispersion efficiency and only requires 30 min sonication to obtain well-dispersed DNA-wrapped individual nanotubes [26]. A longer sonication treatment breaks CNTs and decreases their high aspect ratio [43], which is a property essential to our objective of building percolating networks. Therefore, we chose to make DNA–CNT conjugates with $(GT)_{20}$ repeat units to allow a shorter sonication time. Strands of this length tightly wrap around nanotubes, while a longer DNA strand wraps around nanotubes more loosely and may also entangle multiple nanotubes [44]. We examined both single-walled CNTs (SWNTs) and multi-walled CNTs (MWNTs) in this study. According to the vendor's specifications, the SWNTs have an average diameter of 0.78 nm with a median length of 1 µm. We chose these dimensions because previously reported atomic force microscopy (AFM) studies observed that $(GT)_{20}$ can form multiple wraps around SWNTs with an average diameter around 1 nm [44]. We purchased MWNTs of a much larger size with an average outer diameter of 8.7–10 nm and an average length of 10 µm. The same study showed that DNA wrapping loosens as the nanotubes become larger and mostly only wrap with one turn around MWNTs of greater diameters.

Lastly, we utilized DNA–AuNP conjugates as the fourth type of crosslinker. We synthesized AuNPs with an average diameter of 13 nm using a method adapted from the standard citrate reduction procedure [36]. As-synthesized AuNPs were characterized by TEM, as shown in Figure 2a. DNA–AuNP conjugates were created by attaching ssDNA to the surfaces of AuNPs using the method reported by Zhang et al. [39]. Briefly, 13-nm

AuNPs at neutral pH adsorb DNA strands with polyadenine (A_n) as the anchoring block due to the strong interaction between adenine and gold. We designed a DNA sequence to contain 13-mer of polyadenine (A_{13}) that is connected with a 12-nt sticky end. The polyadenine sequence strongly adsorbed onto AuNPs with high loading capacity. This method produced DNA–AuNP conjugates with much higher concentrations of DNA and AuNPs compared to another method prepared by polymerase chain reaction (PCR) elongation [45].

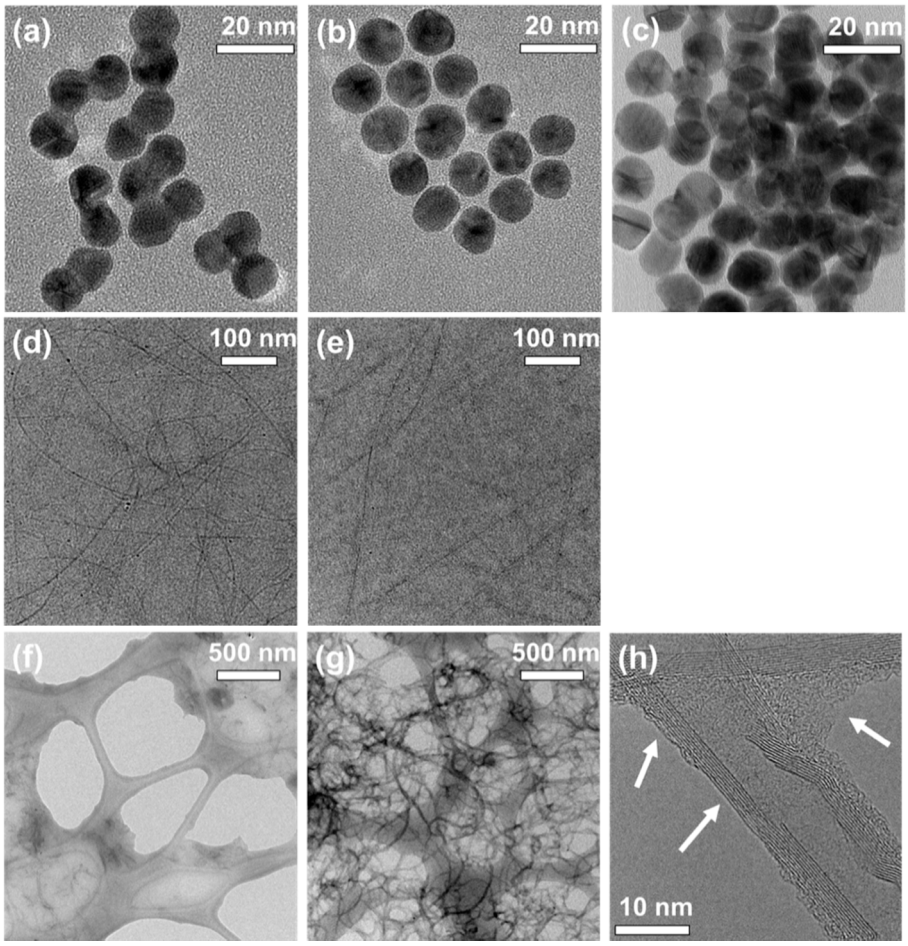

Figure 2. TEM images of (**a**) as-synthesized AuNPs, (**b**) DNA–AuNP conjugates, (**c**) DNA–AuNP hydrogel; (**d**) DNA–single-walled CNT (SWNT) conjugates, (**e**) DNA–SWNT hydrogel; (**f**) DNA–multi-walled CNT (MWNT) conjugates on lacey film, (**g**) DNA–MWNT hydrogel on lacey film, and (**h**) a zoomed-in image of DNA–MWNT hydrogel, showing areas of the CNT wall wrapped by DNA and the bare wall without DNA wrapping. DNA binding between CNT junctions is also shown.

Spacers are linear duplexes formed by two ssDNAs that each contains a sticky end that is complementary to the sticky ends of crosslinkers. We used three different lengths of spacers 33 nt (Ss), 44 nt (Sm), and 55 nt (Sl). The spacer sequences were inspired by Xing et al. [40] and adapted to the other components of our system. All the spacer strands have the same sticky ends that are complementary to the sticky ends on crosslinkers. All the DNA sequences were examined using NUPACK online software (Pasadena, CA, USA) to predict their most stable folded structures to avoid unwanted secondary structures. The final DNA sequences offer a minimum free energy of secondary structure.

3.2. Characterization of Conjugates and Hydrogels

To understand and compare the morphologies of conjugates and hydrogels, we used TEM imaging techniques to visualize AuNP, SWNT, and MWNT conjugates with and

without DNA spacers to show how the crosslinked DNA networks connect and arrange the structures of these nanomaterials. We first imaged the original AuNPs right after synthesis, then the DNA–AuNP conjugates and DNA–AuNP hydrogel constructed by combining DNA–AuNP conjugates with Sl. With the same concept, we also imaged DNA–SWNT conjugates and DNA–MWNT conjugates and then took a look at hydrogels made of these conjugates with the long spacers (Sl). The TEM images of the DNA–CNT hydrogels showed that amorphous materials with hierarchical structures were formed. We can clearly see the larger-scale CNT networks as well as DNA binders on the surfaces of nanotubes, especially around the junctions of CNTs (Figure 2g,h).

3.3. Rheological Properties of DNA Hydrogels

Polymeric hydrogels generally demonstrate robust mechanical strength because of their dense, entangled, and crosslinked networks with small mesh sizes. Unlike these conventional hydrogels, pure DNA hydrogels are more thixotropic and can display poor mechanical strength [46]. Although the mechanical properties of DNA hydrogels can be fine-tuned by adjusting the type and concentration of initial DNA tiles with different numbers of branches, even the toughest DNA hydrogel only exhibits a storage modulus of a few thousand Pa [46]. Because of this property, the applications of DNA hydrogels are limited to only certain fields. To explore further enhancement of DNA hydrogels' mechanical strength, we implemented two strategies: modifying the DNA building blocks and fortifying the structure with novel nanomaterials that confer mechanical rigidity.

We performed small-amplitude oscillatory rheology to understand the gelation properties of pure and DNA hydrogel composites. The storage modulus (G′) and loss modulus (G″) represent the elastic and viscous contributions to the total stress. Viscoelastic materials with solid-like properties are formed due to internal crosslinks within the materials; crosslinking can come from chemical bonds or physical–chemical interactions between individual molecules [47,48].

Using the testing conditions described in the methods session, we performed oscillation measurements on hydrogels formed by Y-shaped DNA tiles, X-shaped DNA tiles, DNA–SWNT conjugates, DNA–MWNT conjugates, and, finally, DNA–AuNP conjugates with spacers of three different lengths. The goals of this group of tests were to study the influence of length of spacers on different types of crosslinkers, as well as to compare the influence of different crosslinkers. For all tested samples, we saw a higher storage modulus (G′) than loss modulus (G″) across the tested angular frequencies, as shown in Figure 3, demonstrating solid-like behavior, which is typically observed for hydrogels constructed with DNA [49,50].

As Figure 3a shows, when constructing pure DNA hydrogels with the same crosslinkers (X or Y), using shorter spacers gives more solid-like hydrogels as indicated by the higher storage modulus. The X-shaped DNA tiles also construct more solid-like hydrogels than the Y-shaped DNA tiles with all types of spacers. However, when using conjugates as crosslinkers (see below), longer spacers construct more solid-like hydrogels, opposite to the behavior observed from pure DNA hydrogels. The mechanical strengths of pure hydrogels are also improved by integrating nanomaterials. With the same spacers (Sl), DNA–SWNT conjugates also construct more solid-like hydrogels than DNA–MWNT conjugates, and both DNA–CNT conjugates make more solid-like hydrogels than DNA–AuNP conjugates (Figure 4).

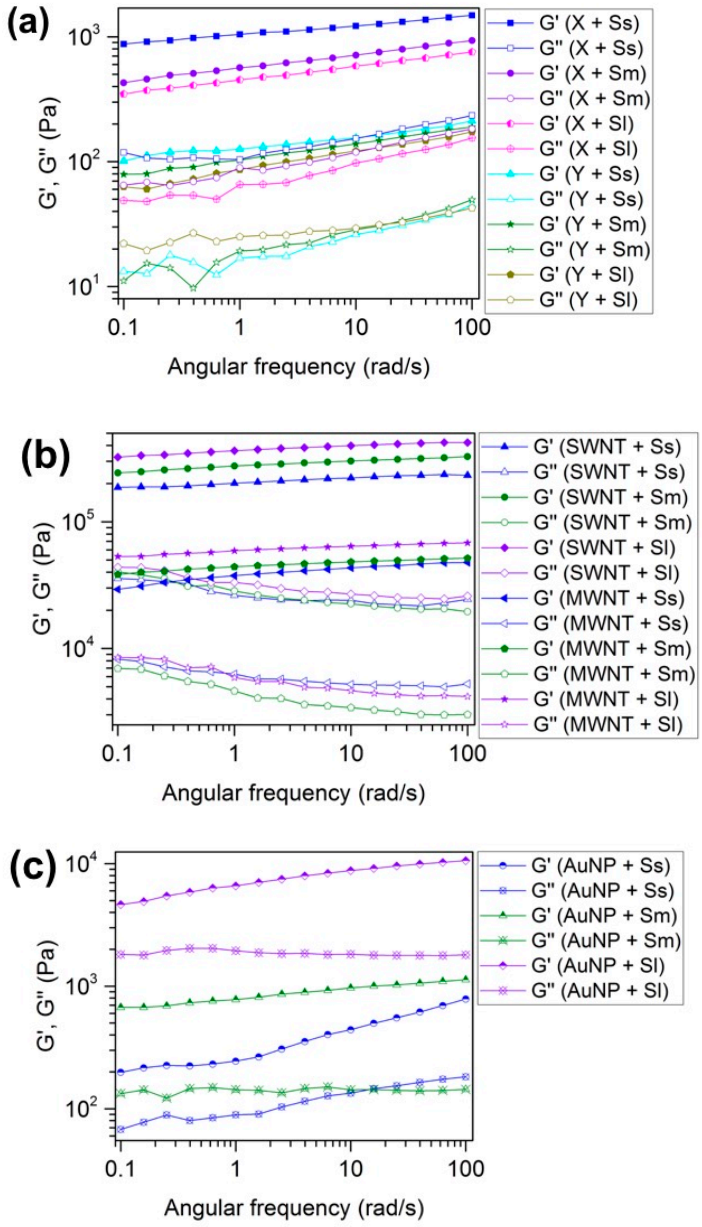

Figure 3. Storage modulus and loss modulus (G′, G″) vs. angular frequencies showing the rheological properties of (**a**) pure DNA hydrogels, (**b**) DNA–SWNT and DNA–MWNT hydrogels, and (**c**) DNA–AuNP hydrogels constructed with spacers of different lengths.

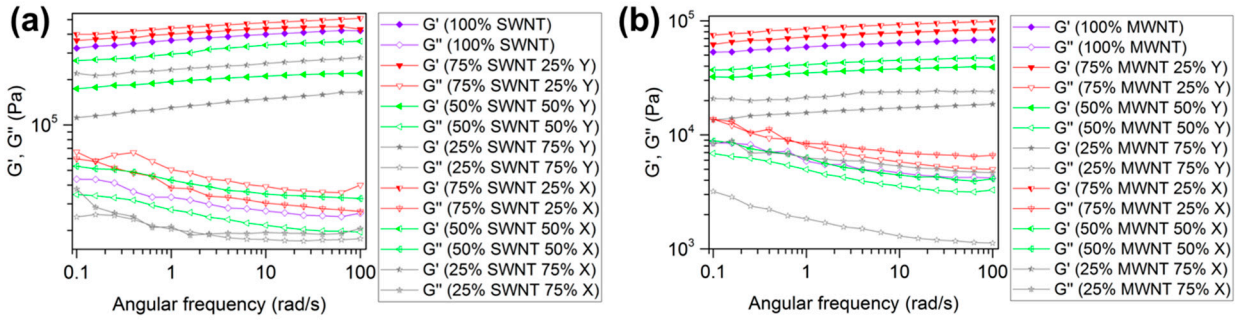

Figure 4. Storage modulus and loss modulus (G′, G″) vs. angular frequencies showing the rheological properties of (**a**) hydrogel composites constructed with DNA–SWNT conjugates, X- (or Y-) shaped DNA tiles, and long spacer (Sl); and (**b**) hydrogel composites constructed with DNA–MWNT conjugates, X- (or Y-) shaped DNA tiles, and Sl.

Our next set of tests was to use mixed crosslinkers, combining DNA–CNT conjugates and DNA tiles. The objective of these tests was to show the influence of different crosslinker compositions and to see how mixed crosslinkers of different length scales change the mechanical properties of the final hydrogels. Specifically, we substituted 25%, 50%, and 75% of the DNA–CNT conjugates from the previous test with X- or Y-shaped DNA tiles while keeping the total concentration of sticky ends from all crosslinkers the same. Only long spacer (Sl) was used for these mixed crosslinker tests. The oscillatory measurements showed that hydrogels constructed using Sl and containing a crosslinker mixture of 75% DNA–CNT conjugates and 25% DNA tiles exhibited the highest values of G'. This composition formed hydrogels with G' above 50 kPa, over 100-fold higher than the G' of pure DNA hydrogels. It is followed by using Sl with 100% DNA–CNT conjugates as crosslinkers. Then, the mechanical strength dropped even further when using Sl with 50% DNA–CNT conjugates and 50% DNA tiles crosslinkers, and hydrogels constructed by Sl with 25% DNA–CNT conjugates and 75% DNA tiles had the lowest storage modulus. All DNA hydrogel composites still had higher mechanical strengths than pure DNA hydrogels. Moreover, using DNA–SWNT conjugates always gave more solid-like hydrogels than using DNA–MWNT conjugates in the above compositions, and using X-shaped DNA tiles resulted in more solid-like hydrogels than using Y-shaped DNA tiles in these compositions.

3.4. Electrical Characterization

In order to minimize undesired complications due to ionic conduction associated with performing electrical measurements on nanocircuits embedded within hydrogels, we performed two-dimensional measurements of dehydrated hydrogels instead. We used a two-terminal current–voltage (IV) characterization setup with parallel line-shaped gold electrodes. As shown in Figure S5, the gold microelectrodes were fabricated with 200 µm spacing and were wire-bonded to a commercial ball grid array (BGA) board connected to the setup. The hydrogel was placed across the gap between microelectrodes and then dried completely before IV curves were recorded. IV characterization allows the measurement of small conductivity as a response to an applied voltage. During the test, the current was measured during 10 consecutive pulses of 10 V. The goal of IV characterization is to investigate whether or not DNA crosslinking creates more organized or clumpy networks based on the changes in conductivity after adding spacers to the conjugates.

As shown in Figure 5a, dehydrated samples of DNA–SWNT conjugates and DNA–SWNT hydrogel both showed non-linear behaviors. With the same applied voltage pulses, the measured current increased greatly in the hydrogel samples with spacers compared to DNA–SWNT conjugates—over a 650-fold increase. Since MWNTs are highly conductive, they showed a wire-like behavior with a much higher conductivity compared to the SWNT samples. In the MWNT case, adding DNA spacers also increased the conductivity of DNA–MWNT conjugates by 45-fold—see Figure 5b. When testing with DNA–AuNP samples, the current increased four-fold after adding spacers to the conjugates and forming gel-like networks, as shown in Figure 5c.

These electrical measurements demonstrate that modification and organization of nanomaterials using DNA strands can be used to control the electrical behavior of percolating networks and can change the conductivity of composites by using DNA self-assembly to connect the nanomaterials.

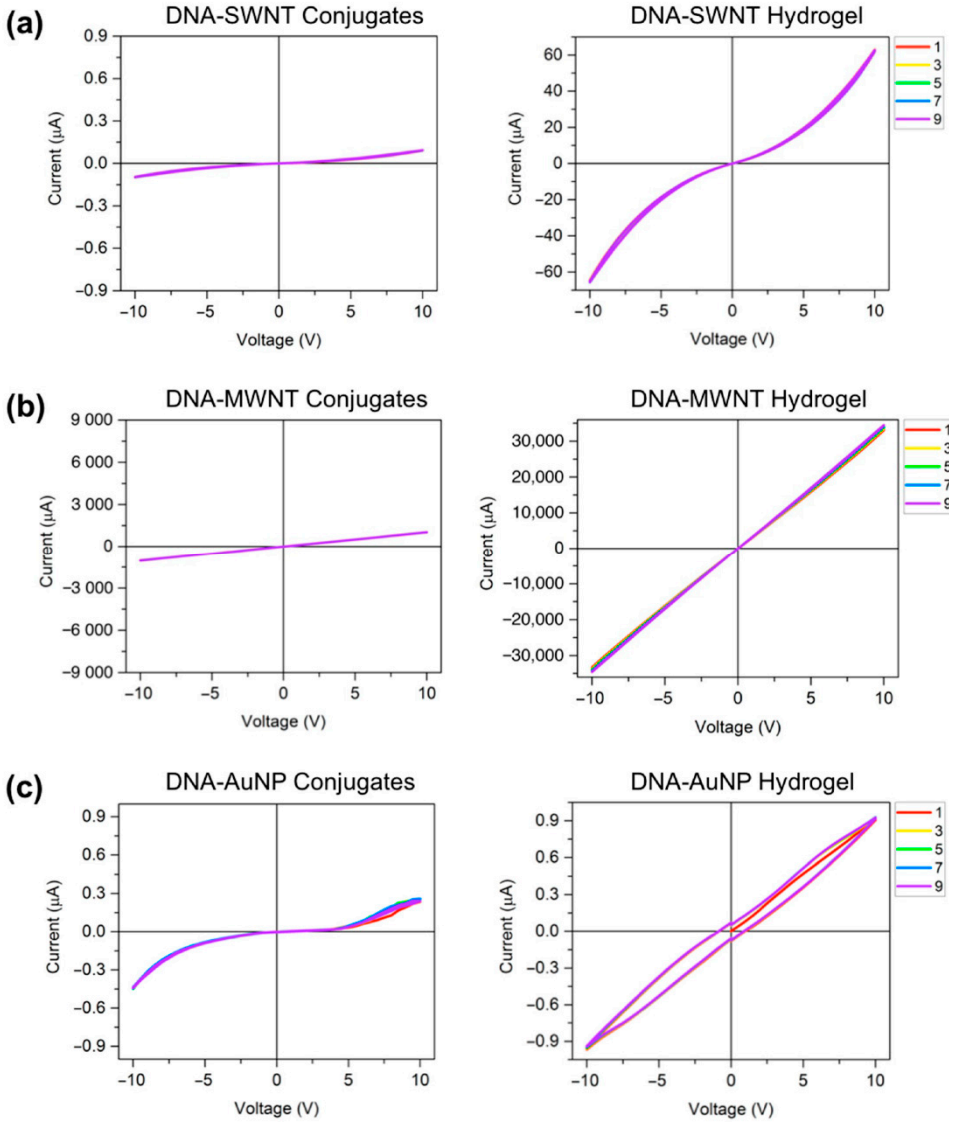

Figure 5. Current–voltage (IV) curves of dehydrated samples. (**a**) DNA–SWNT conjugates (left) vs. DNA–SWNT hydrogel (right); (**b**) DNA–MWNT conjugates (left) vs. DNA–MWNT hydrogel (right); (**c**) DNA–AuNP conjugates (left) vs. DNA–AuNP hydrogel (right). All measured across gold electrodes with 200 μm spacings. Legend shows pulse number.

4. Discussion

4.1. Characterizations

We first characterized citrate-stabilized AuNPs with TEM, demonstrating that synthesized nanoparticles were homogeneous and that their average diameter was 13.1 ± 1.8 nm (Figure 2a and Figure S3). As-synthesized AuNPs appeared clustered in groups of two or three, with no clear spaces between individual nanoparticles within the groups. However, the images of DNA–AuNP conjugates showed that DNA-attached AuNPs have a clear and much more uniform spacing between neighboring particles, which was measured to have an average of 0.78 nm (Figure 2b). By comparing the morphologies of AuNP clustering in Figure 2a,b, we showed that DNA strands modified the surfaces of AuNPs. We further characterized DNA–AuNP conjugates using gel electrophoresis. Non-DNA-attached AuNPs aggregated in the well and failed to enter the gel. DNA-modified AuNPs did not aggregate and were able to migrate into the gel (as shown in Figure S4). The TEM images agreed with the gel electrophoresis results and demonstrated that we successfully decorated AuNPs with ssDNA. Next, we constructed DNA–AuNP hydrogel composites by combining DNA–AuNP conjugates and long spacers (Sl). We further confirmed the

formation of hydrogel composites by characterization of a hydrogel sample using TEM (Figure 2c). The TEM images showed multiple layers of AuNPs on top of each other that appeared to be held together during sample collapse from drying. Comparing that with Figure 2b, it is apparent that DNA spacers had linked AuNPs together in a 3D structure.

Although differences in clustering and morphology between DNA–SWNT in conjugates versus hydrogel are not entirely distinctive using TEM characterization (Figure 2d,e), the differences were apparent in the MWNT samples (Figure 2f,g). DNA–MWNT conjugates appeared to gather on the lacy carbon film on the copper grids and did not appear to fill in most holes in the film. On the other hand, the dehydrated hydrogel made of DNA–MWNT conjugates with long spacers (Sl) covered the entire lacy film (including holes in the film) with its own networks formed by the nanotubes. DNA spacers helped to connect MWNTs together into a web-like structure over a large area. When taking a closer look at individual MWNTs, we observed regions of coating over the nanotubes, with an average thickness of 1.51 nm. Figure 2h clearly shows that the middle area of the MWNT was not wrapped by DNA, while the areas close to MWNT junctions were coated. Figure 2h also shows a thicker coating around MWNT junctions, indicating the location of spacers. These images represent a direct observation of DNA acting as a "smart" glue to bind and connect MWNTs together. Overall, we successfully constructed pure DNA hydrogels and DNA hydrogel composites with nanomaterials.

4.2. Rheological Results

We would like to construct hydrogels of reasonable mechanical strength where the crosslinked networks can effectively prevent diffusion of the nanomaterials and, thus, to achieve hydrogels with confined architecture for further applications. Having a higher storage modulus than loss modulus from oscillation frequency tests indicated that we indeed made hydrogels with solid-like properties. When using the same DNA tiles as crosslinkers, we observed that shorter spacers constructed hydrogels of higher mechanical strengths as they are able to build a denser network. The situation is reversed and longer spacers constructed more solid-like hydrogels when using DNA/nanomaterial conjugates as crosslinkers. This is because the CNTs and AuNPs we used are much larger in scale compared to DNA molecules; thus, having longer spacers helped to build more and more stable bridges between nanomaterial/crosslinker components. Therefore, we used Sl for all electrical studies and structural characterization analysis.

CNTs are well known for their mechanical reinforcement applications. Consistent with previous observations in other composites, we observed a huge increase in storage modulus with DNA–CNT hydrogel composites compared to pure DNA hydrogels. When using one type of crosslinker, DNA–SWNT conjugates constructed the most solid-like hydrogels, followed by using DNA–MWNT conjugates, DNA–AuNP conjugates, X-shaped DNA tiles, and, finally, Y-shaped DNA tiles. We believe that we observed a higher storage modulus from hydrogels constructed with DNA–SWNT conjugates than hydrogels constructed with DNA–MWNT conjugates because DNA wraps around SWNTs more tightly with more turns [51]. The TEM images (Figure 2) also showed that DNA coats on SWNTs much better than on MWNTs. As the average diameter of CNTs increases from SWNTs (0.78 nm) to MWNTs (~9 nm), $(GT)_{20}$ loses its strong binding around the nanotubes, which resulted in a decrease in mechanical performance of hydrogels made with these conjugates. This result shows the importance of crosslinked DNA as the binding material to connect nanomaterials and to build networks. Furthermore, hydrogels constructed with both types of DNA–CNT conjugate crosslinkers showed higher mechanical strength than hydrogels constructed with DNA–AuNP conjugates because the high aspect ratios of CNTs are inherently in favor of providing reinforcement to composites compared to sphere-shaped materials.

We further investigated and rationally improved the mechanical properties of hybrid hydrogels by combining DNA/nanomaterial conjugates and DNA tiles as crosslinkers. Since CNTs and AuNPs are in much larger scales than DNA molecules, there are available spaces between individual nanotubes and nanoparticles in the hydrogels, where there is

no DNA filling besides the DNA network associated with binding strands and spacers. These hydrogels have the capacity to integrate more materials that can fill in the spaces. Therefore, we used different compositions of DNA/nanomaterial conjugates and DNA tiles to construct hydrogels in which crosslinkers come in different scales. When we used DNA tiles to make up to 25% of crosslinkers and DNA–CNT conjugates for the rest, the resulted hydrogels were even more solid-like than when using 100% DNA–CNT conjugates as crosslinkers. This is because substituting some of the DNA–CNT conjugates with a much smaller type of crosslinkers helped to fill in the open spaces between CNTs and, thus, made a denser hydrogel. However, DNA molecules are significantly weaker than CNTs, so we observed a decrease in mechanical strength when substituting more DNA–CNT conjugates with DNA tiles. In summary, we demonstrated adjustment of the mechanical properties of hybrid hydrogels by combining different compositions of crosslinkers and achieved the most solid-like hydrogel when using DNA–CNT conjugates as 75% of crosslinkers and X-shaped DNA tiles for the remaining 25% of crosslinkers.

4.3. Electrical Studies

Studies on the conductivity of DNA mostly agree that DNA is not a good conductor and does not contribute to conductivity in composites when conductive nanomaterials are present [51]. However, DNA has been seen as a good candidate to self-organize nanocircuits into a complex system. Therefore, besides mechanical reinforcement, another objective of integrating nanomaterials into the hydrogel composites is to modify the electrical behavior and add functionality to the hydrogels. For this reason, we used semiconducting SWNTs when making DNA–SWNT conjugates. In a previous electrical study of a single SWNT on parallel gold electrodes [52], the IV curves showed a saturation of conductance at high voltages. We did not observe such a saturation from IV characterization of SWNT networks from conjugates and hydrogels (Figure 5a).

Circuits built with AuNPs have a lower conductivity compared to the ones created with CNTs, since the nanosphere structure does not have the advantage in reaching long-range percolation as nanotubes of much greater aspect ratios do. For the same reason, adding spacers to DNA–AuNP conjugates also does not result in as much of an enhancement in conductivity. This result showed that the shape of nanomaterials needs to be considered when designing hydrogels to ensure that the assembled circuits have the desired performance. Increased control of the architectural characteristics of percolation paths formed by CNTs and AuNPs (i.e., length scale, clumpiness, subcircuit structures, etc.) will encourage further investigation of these embedded networks for potential applications in neuromorphic and error-tolerant computing.

5. Conclusions

We designed and built pure DNA hydrogels as well as composites using DNA/nanomaterial conjugate crosslinkers, DNA tile crosslinkers, and linear DNA spacers. We characterized the nanomaterial networks in the composites and examined their mechanical and electrical behaviors. We found that shorter spacers form more solid-like hydrogels when combined with pure DNA crosslinkers, while longer spacers construct more solid-like hydrogels when assembled with DNA/nanomaterial crosslinkers. We obtained hydrogel composites with significantly higher mechanical strength by combining DNA–CNT conjugates and up to 25% DNA tiles as crosslinkers. In addition, dried networks from both DNA–SWNT and DNA–AuNP conjugates and hydrogels show non-linear electrical behaviors. By comparing the conductivities of dehydrated networks from conjugates and hydrogels, we showed the ability of DNA self-assembly to integrate and connect percolating networks with nanotubes and nanoparticles. These initial examples of biomolecular functionality by design suggest that the basic concepts of DNA self-assembly can effectively be used to create more complicated materials. Potentially, crosslinkers such as DNA-wrapped CNTs can be used to create more sophisticated conjugates and nanostructures. We can design DNA to realize control in nanoelectronics morphology through connection and

arrangement of nanomaterials. These materials have potential for applications in 3D integrated circuits and hardware with shorter production time, lower cost, lower power consumption, and higher energy efficiency. Eventually, electronic hardware utilizing 3D integration and assembled using DNA nanotechnology may achieve computing capabilities in certain operations beyond the performance currently achieved by circuits fabricated using traditional lithography techniques.

Supplementary Materials: The following are available online at https://www.mdpi.com/2076-3417/11/5/2245/s1, Figure S1: Photos of (a) SWNT and (b) MWNT dispersions in deionized (DI) water without (left) and with (right) DNA modification. SWNTs and MWNTs without DNA modification settle at the bottom within 15 min after sonication; Figure S2: Photos of pure and DNA hydrogel composites constructed by Sl with (from left to right) Y-shaped DNA tiles, X-shaped DNA tiles, DNA–SWNT conjugates, DNA–MWNT conjugates, and DNA–AuNP conjugates; Figure S3: UV–Vis spectrum of as-synthesized AuNPs. A peak λ_{max} at 519 nm wavelength proves that these are well-formed AuNPs with an average diameter of 13 nm. UV–Vis spectrum was recorded on a Thermo Scientific NanoDrop 2000c Spectrophotometer (Waltham, USA); Figure S4: The band of pure AuNPs (left) appears violet under visible light, while the band of DNA–AuNP conjugates (right) retains a red color and shows a much better mobility; Figure S5: Gold electrodes of 200 µm spacing for electrical characterization; Table S1: Sequences of ssDNA for the preparation of crosslinkers and spacers; Table S2: Concentrations and ratios of crosslinkers and spacers to prepare for hydrogel.

Author Contributions: Conceptualization, T.H.L., A.K., and M.G.; methodology, T.H.L., A.K., L.C.H., and M.G.; formal analysis, M.G., A.M., and A.K.; investigation, M.G., A.M., and A.K.; Writing—Original draft preparation, M.G.; Writing—Review and editing, M.G., A.K., T.H.L., L.C.H., and A.M. All authors have read and agreed to the published version of the manuscript.

Funding: This research was partially funded by the US National Science Foundation through grant NSF-CISE-CCF 1748459 to T.H.L.

Institutional Review Board Statement: Not Applicable.

Informed Consent Statement: Not Applicable.

Acknowledgments: The authors thank E. Vetter, M. Hart, and C. Winkler for help with experiments. This work was performed in part at the Analytical Instrumentation Facility (AIF) at North Carolina State University, which is supported by the State of North Carolina and the National Science Foundation (award number ECCS-2025064). The AIF is a member of the North Carolina Research Triangle Nanotechnology Network (RTNN), a site in the National Nanotechnology Coordinated Infrastructure (NNCI).

Conflicts of Interest: The authors declare no conflict of interest.

References

1. Winfree, E.; Liu, F.; Wenzler, L.A.; Seeman, N.C. Design and self-assembly of two-dimensional DNA crystals. *Nature* **1998**, *394*, 539–544. [CrossRef]
2. Rothemund, P.W.K. Folding DNA to create nanoscale shapes and patterns. *Nature* **2006**, *440*, 297–302. [CrossRef] [PubMed]
3. Douglas, S.M.; Dietz, H.; Liedl, T.; Högberg, B.; Graf, F.; Shih, W.M. Self-assembly of DNA into nanoscale three-dimensional shapes. *Nature* **2009**, *459*, 414–418. [CrossRef]
4. Marchi, A.N.; Saaem, I.; Vogen, B.N.; Brown, S.; LaBean, T.H. Toward Larger DNA Origami. *Nano Lett.* **2014**, *14*, 5740–5747. [CrossRef]
5. Wagenbauer, K.F.; Sigl, C.; Dietz, H. Gigadalton-scale shape-programmable DNA assemblies. *Nature* **2017**, *552*, 78–83. [CrossRef]
6. Yan, H.; Park, S.H.; Finkelstein, G.; Reif, J.H.; LaBean, T.H. DNA-Templated Self-Assembly of Protein Arrays and Highly Conductive Nanowires. *Science* **2003**, *301*, 1882–1884. [CrossRef] [PubMed]
7. Knudsen, J.; Liu, L.; Kodal, A.; Madsen, M.; Li, Q.; Song, J.; Woehrstein, J.; Wickham, S.; Strauss, M.; Schueder, F.; et al. Routing of individual polymers in designed patterns. *Nat. Nanotechnol.* **2015**, *10*, 892–898. [CrossRef]
8. Krissanaprasit, A.; Madsen, M.; Knudsen, J.B.; Gudnason, D.A.; Surareungchai, W.; Birkedal, V.; Gothelf, K.V. Programmed Switching of Single Polymer Conformation on DNA Origami. *ACS Nano* **2016**, *10*, 2243–2250. [CrossRef] [PubMed]
9. Madsen, M.; Christensen, R.S.; Krissanaprasit, A.; Bakke, M.R.; Riber, C.F.; Nielsen, K.S.; Zelikin, A.N.; Gothelf, K.V. Preparation, Single-Molecule Manipulation, and Energy Transfer Investigation of a Polyfluorene-graft -DNA polymer. *Chem. A Eur. J.* **2017**, *23*, 10511–10515. [CrossRef]

10. Shahbazi, M.-A.; Bauleth-Ramos, T.; Santos, H.A. DNA Hydrogel Assemblies: Bridging Synthesis Principles to Biomedical Applications. *Adv. Ther.* **2018**, *1*, 1800042. [CrossRef]
11. Li, F.; Lyu, D.; Liu, S.; Guo, W. DNA Hydrogels and Microgels for Biosensing and Biomedical Applications. *Adv. Mater.* **2020**, *32*, e1806538. [CrossRef]
12. Lee, J.B.; Peng, S.; Yang, D.; Roh, Y.H.; Funabashi, H.; Park, N.; Rice, E.J.; Chen, L.; Long, R.; Wu, M.; et al. A mechanical metamaterial made from a DNA hydrogel. *Nat. Nanotechnol.* **2012**, *7*, 816–820. [CrossRef] [PubMed]
13. Liu, H.; Cao, T.; Xu, Y.; Dong, Y.; Liu, D. Tuning the Mechanical Properties of a DNA Hydrogel in Three Phases Based on ATP Aptamer. *Int. J. Mol. Sci.* **2018**, *19*, 1633. [CrossRef] [PubMed]
14. Khajouei, S.; Ravan, H.; Ebrahimi, A. DNA hydrogel-empowered biosensing. *Adv. Colloid Interface Sci.* **2020**, *275*, 102060. [CrossRef] [PubMed]
15. Thelu, H.V.P.; Atchimnaidu, S.; Perumal, D.; Harikrishnan, K.S.; Vijayan, S.; Varghese, R. Self-Assembly of an Aptamer-Decorated, DNA—Protein Hybrid Nanogel: A Biocompatible Nanocarrier for Targeted Cancer Therapy. *ACS Appl. Bio Mater.* **2019**, *2*, 5227–5234. [CrossRef]
16. Gačanin, J.; Synatschke, C.V.; Weil, T. Biomedical Applications of DNA-Based Hydrogels. *Adv. Funct. Mater.* **2020**, *30*, 1906253. [CrossRef]
17. Cheng, E.; Xing, Y.; Chen, P.; Yang, Y.; Sun, Y.; Zhou, D.; Xu, L.; Fan, Q.; Liu, D. A pH-Triggered, Fast-Responding DNA Hydrogel. *Angew. Chem. Int. Ed.* **2009**, *48*, 7660–7663. [CrossRef] [PubMed]
18. Li, C.; Faulkner-Jones, A.; Dun, A.R.; Jin, J.; Chen, P.; Xing, Y.; Yang, Z.; Li, Z.; Shu, W.; Liu, D.; et al. Rapid Formation of a Supramolecular Polypeptide-DNA Hydrogel for In Situ Three-Dimensional Multilayer Bioprinting. *Angew. Chem. Int. Ed.* **2015**, *54*, 3957–3961. [CrossRef]
19. Zhou, D.; Ying, L.; Hong, X.; Hall, E.A.; Abell, C.; Klenerman, D. A Compact Functional Quantum Dot—DNA Conjugate: Preparation, Hybridization, and Specific Label-Free DNA Detection. *Langmuir* **2008**, *24*, 1659–1664. [CrossRef]
20. Hurst, S.J.; Lytton-Jean, A.K.R.; Mirkin, C.A. Maximizing DNA Loading on a Range of Gold Nanoparticle Sizes. *Anal. Chem.* **2006**, *78*, 8313–8318. [CrossRef] [PubMed]
21. Li, Z.; Wu, Z.; Li, K. The high dispersion of DNA—multiwalled carbon nanotubes and their properties. *Anal. Biochem.* **2009**, *387*, 267–270. [CrossRef]
22. Hu, Y.; Domínguez, C.M.; Bauer, J.; Weigel, S.; Schipperges, A.; Oelschlaeger, C.; Willenbacher, N.; Keppler, S.; Bastmeyer, M.; Heißler, S.; et al. Carbon-nanotube reinforcement of DNA-silica nanocomposites yields programmable and cell-instructive biocoatings. *Nat. Commun.* **2019**, *10*, 1–14. [CrossRef]
23. Kyrylyuk, A.V.; Hermant, M.C.; Schilling, T.; Klumperman, B.; Koning, C.E.; van der Schoot, P. Controlling electrical percolation in multicomponent carbon nanotube dispersions. *Nat. Nanotechnol.* **2011**, *6*, 364–369. [CrossRef]
24. Vardharajula, S.; Ali, S.Z.; Tiwari, P.M.; Eroğlu, E.; Vig, K.; Dennis, V.A.; Singh, S.R. Functionalized carbon nanotubes: Biomedical applications. *Int. J. Nanomed.* **2012**, *7*, 5361–5374. [CrossRef]
25. Nakashima, N.; Okuzono, S.; Murakami, H.; Nakai, T.; Yoshikawa, K. DNA Dissolves Single-walled Carbon Nanotubes in Water. *Chem. Lett.* **2003**, *32*, 456–457. [CrossRef]
26. Zheng, M.; Jagota, A.; Semke, E.D.; Diner, B.A.; McLean, R.S.; Lustig, S.R.; Richardson, R.E.; Tassi, N.G. DNA-assisted dispersion and separation of carbon nanotubes. *Nat. Mater.* **2003**, *2*, 338–342. [CrossRef] [PubMed]
27. Dovbeshko, G.; Repnytska, O.; Obraztsova, E.; Shtogun, Y. DNA interaction with single-walled carbon nanotubes: A SEIRA study. *Chem. Phys. Lett.* **2003**, *372*, 432–437. [CrossRef]
28. Chen, Y.; Liu, H.; Ye, T.; Kim, A.J.; Mao, C. DNA-Directed Assembly of Single-Wall Carbon Nanotubes. *J. Am. Chem. Soc.* **2007**, *129*, 8696–8697. [CrossRef] [PubMed]
29. Rueckes, T.; Kim, K.; Joselevich, E.; Tseng, G.Y.; Cheung, C.-L.; Lieber, C.M. Carbon Nanotube-Based Nonvolatile Random Access Memory for Molecular Computing. *Science* **2000**, *289*, 94–97. [CrossRef]
30. Kang, J.W.; Lee, J.H.; Lee, H.J.; Hwang, H.J. A study on carbon nanotube bridge as a electromechanical memory device. *Phys. E Low Dimens. Syst. Nanostruct.* **2005**, *27*, 332–340. [CrossRef]
31. Li, D.; Song, S.; Fan, C. Target-Responsive Structural Switching for Nucleic Acid-Based Sensors. *Acc. Chem. Res.* **2010**, *43*, 631–641. [CrossRef]
32. Lin, C.; Liu, Y.; Yan, H. Designer DNA Nanoarchitectures. *Biochemistry* **2009**, *48*, 1663–1674. [CrossRef] [PubMed]
33. Mirkin, C.A.; Letsinger, R.L.; Mucic, R.C.; Storhoff, J.J. A DNA-based method for rationally assembling nanoparticles into macroscopic materials. *Nature* **1996**, *382*, 607–609. [CrossRef] [PubMed]
34. Alivisatos, A.P.; Johnsson, K.P.; Peng, X.; Wilson, T.E.; Loweth, C.J.; Bruchez, M.P.; Schultz, P.G. Organization of 'nanocrystal molecules' using DNA. *Nature* **1996**, *382*, 609–611. [CrossRef]
35. Storhoff, J.J.; Elghanian, R.; Mirkin, C.A.; Letsinger, R.L. Sequence-Dependent Stability of DNA-Modified Gold Nanoparticles. *Langmuir* **2002**, *18*, 6666–6670. [CrossRef]
36. Hill, H.D.; Mirkin, C.A. The bio-barcode assay for the detection of protein and nucleic acid targets using DTT-induced ligand exchange. *Nat. Protoc.* **2006**, *1*, 324–336. [CrossRef] [PubMed]
37. Haiss, W.; Thanh, N.T.K.; Aveyard, J.; Fernig, D.G. Determination of Size and Concentration of Gold Nanoparticles from UV—Vis Spectra. *Anal. Chem.* **2007**, *79*, 4215–4221. [CrossRef] [PubMed]
38. Cheng, E.; Li, Y.; Yang, Z.; Deng, Z.; Liu, D. DNA-SWNT hybrid hydrogel. *Chem. Commun.* **2011**, *47*, 5545–5547. [CrossRef]

39. Zhang, X.; Liu, B.; Dave, N.; Servos, M.R.; Liu, J. Instantaneous Attachment of an Ultrahigh Density of Nonthiolated DNA to Gold Nanoparticles and Its Applications. *Langmuir* **2012**, *28*, 17053–17060. [CrossRef]
40. Xing, Y.; Cheng, E.; Yang, Y.; Chen, P.; Zhang, T.; Sun, Y.; Yang, Z.; Liu, D. Self-Assembled DNA Hydrogels with Designable Thermal and Enzymatic Responsiveness. *Adv. Mater.* **2010**, *23*, 1117–1121. [CrossRef]
41. Um, S.H.; Lee, J.B.; Park, N.; Kwon, S.Y.; Umbach, C.C.; Luo, D. Enzyme-catalysed assembly of DNA hydrogel. *Nat. Mater.* **2006**, *5*, 797–801. [CrossRef] [PubMed]
42. Zheng, M.; Jagota, A.; Strano, M.S.; Santos, A.P.; Barone, P.; Chou, S.G.; Diner, B.A.; Dresselhaus, M.S.; McLean, R.S.; Onoa, G.B.; et al. Structure-Based Carbon Nanotube Sorting by Sequence-Dependent DNA Assembly. *Science* **2003**, *302*, 1545–1548. [CrossRef] [PubMed]
43. Lahiji, R.R.; Dolash, B.D.; Bergstrom, D.E.; Reifenberger, R. Oligodeoxyribonucleotide Association with Single-Walled Carbon Nanotubes Studied by SPM. *Small* **2007**, *3*, 1912–1920. [CrossRef] [PubMed]
44. Yang, Q.-H.; Wang, Q.; Gale, N.; Oton, C.J.; Cui, L.; Nandhakumar, I.S.; Zhu, Z.; Tang, Z.; Brown, T.; Loh, W.H. Loosening the DNA wrapping around single-walled carbon nanotubes by increasing the strand length. *Nanotechnology* **2009**, *20*, 195603. [CrossRef]
45. Eguchi, Y.; Kato, T.; Tanaka, T.; Maruyama, T. A DNA–gold nanoparticle hybrid hydrogel network prepared by enzymatic reaction. *Chem. Commun.* **2017**, *53*, 5802–5805. [CrossRef]
46. Li, F.; Tang, J.; Geng, J.; Luo, D.; Yang, D. Polymeric DNA hydrogel: Design, synthesis and applications. *Prog. Polym. Sci.* **2019**, *98*, 101163. [CrossRef]
47. Chambon, F.; Winter, H.H. Linear Viscoelasticity at the Gel Point of a Crosslinking PDMS with Imbalanced Stoichiometry. *J. Rheol.* **1987**, *31*, 683–697. [CrossRef]
48. Cardenas-Vasquez, E.D.; Smith, K.M.; Doolan, T.J.; Hsiao, L.C. Shear-Induced Microstructural Variations in Nanoemulsion-Laden Organohydrogel Fibers. *ACS Appl. Polym. Mater.* **2019**, *2*, 594–603. [CrossRef]
49. Nöll, T.; Schönherr, H.; Wesner, D.; Schopferer, M.; Paululat, T.; Nöll, G. Construction of Three-Dimensional DNA Hydrogels from Linear Building Blocks. *Angew. Chem. Int. Ed.* **2014**, *53*, 8328–8332. [CrossRef]
50. Jiang, H.; Pan, V.; Vivek, S.; Weeks, E.R.; Ke, Y. Programmable DNA Hydrogels Assembled from Multidomain DNA Strands. *ChemBioChem* **2016**, *17*, 1156–1162. [CrossRef]
51. Campbell, J.F.; Tessmer, I.; Thorp, H.H.; Erie, D.A. Atomic Force Microscopy Studies of DNA-Wrapped Carbon Nanotube Structure and Binding to Quantum Dots. *J. Am. Chem. Soc.* **2008**, *130*, 10648–10655. [CrossRef] [PubMed]
52. Navarro, C.G.; de Pablo, P.; Herrero, J.G. Electrical properties of long molecules: Single-walled carbon nanotubes and DNA. *Int. J. Nanotechnol.* **2005**, *2*, 90. [CrossRef]